Dalton Transactions

Accepted Manuscript

ROYAL SOCIETY OF CHEMISTRY

www.rsc.org/dalton

Journal Name

Dalton Transactions

Morphology-controlled MnO_2-Graphene Oxides-Diatomaceous Earth 3-dimensional (3D) Composites for High-performance Supercapacitors

Received 00th January 20xx,
Accepted 00th January 20xx

DOI: 10.1039/x0xx00000x

www.rsc.org/

Zhong Quan Wen[a,*], Min Li[a], Fei Li[b], Shi Jin Zhu[b], Xiao Ying Liu[b], Yu Xin Zhang[a,b*], Tushar Kumeria[c], Dusan Losic[c,*], Yang Gao[d], Wei Zhang[e], Shi Xuan He[e]

The 3-dimensional (3D) composites based on unique combination of MnO_2-nanostrctures, graphene oxide nanosheets and porous Diatomaceous Earth (DE) microparticles (GO-DE@MnO_2) were synthesized and explored for high-performance supercapacitors. To explore influence of the structural properties of MnO_2 nanostructures on supercapacitor performances several MnO_2 structures with nanosheets and nanowires morphology were synthetized and characterized. The prepared GO-DE@MnO_2 composites with MnO_2 nanosheets due to their higher conductivity and higher surface area showed the larger specific capacitance of 152.5 F g^{-1} and the relatively better cycle stability (83.3% capacitance retention after 2000 cycles at the scan rate of 2 A g^{-1}), signifying a great potential application for supercapacitors.

Keywords: diatomaceous earth; manganese dioxide; core-shell nanostructures; supercapacitors

Introduction

To fulfill the requirements for energy storage, supercapacitors, as a traditional source of on-demand power, are attracting worldwide attention. They are the most promising candidates for next-generation energy devices due to their long cycle life, high power density, high specific capacitance, environment benignity and good stability [1-4]. According to the energy storage mechanism, supercapacitors are normally divided into electrochemical double layer capacitors (EDLC), using carbon-active materials (e.g., CNT, graphene) based on the surface area of the electrode materials [5-8], and pseudocapacitors, using redox-active materials based on the fast and reversible Faradic reactions [3]. The specific capacitance just from the electrical charges at the electrode-electrolyte interface of EDLC is lower than pseudocapacitance, such as transition metal oxides [9-12] and conducting polymers [13,14,16].

Due to the high theoretical specific capacitance (1370 F g^{-1}), low cost, environmental friendliness and wide operating potential window in mild electrolyte [9,15,17], manganese dioxide (MnO_2) has been extensively recognized as a supercapacitor electrode material. To date, manganese oxides with various structures and morphologies have been fabricated via electrochemical and chemical routes, and their electrochemical properties have been studied [18,19]. Nevertheless, manganese oxide electrodes have poor electrical conductivity which has surely impeded the emersion of capacity, leading to a poor rate capability [20,21].

As a matter of fact, the electrochemical capacitance of MnO_2 can be significantly improved by combining MnO_2 with carbonaceous materials [3,21]. Their supercapacitance performance were significantly improved when these composites were designed as 3-dimensional (3D) composites with increased surface area. Following this strategy in this work we made new 3D composites material by combining MnO_2 nanostructuers, graphene oxide nanoheets with natural porous 3D diatom silica microparticles. The idea here was to use unique hollow and mesoporous structure of diatoms microparticles and combine them with 2D GO sheets and MnO_2 nanostructures to build for the first time unique 3D composite we propose should have adavnaced supercapacitor performances. The schematic diagram showing our concept and preparation process is illustrated in Fig. 1. Using simple hydrothermal method, we synthesized the GO-DE@MnO_2 3D composites with two forms of

[a] College of Optoelectronic Engineering, Key Laboratory of Fundamental Science of Micro/Nano-Devices and System Technology, Chongqing University, Chongqing 400044, PR China
[b] College of Materials Science and Engineering, Chongqing University, Chongqing 400044, PR China
[c] School of Chemical Engineering, The University of Adelaide, Adelaide, SA 5005, Australia
[d] Institute of Electronic Engineering, China Academy of Engineering Physics, Mianyang 621900, PR China
[e] Chongqing Institute of Green and Intelligent Technology, Chinese Academy of Sciences, Chongqing 400714, PR China

*E-mail: wenzq@cqu.edu.cn; zhangyuxin@cqu.edu.cn; dusan.losic@adelaide.edu.au
Fax: +86-23 6510 4131; Tel: +86-23 6510 4131

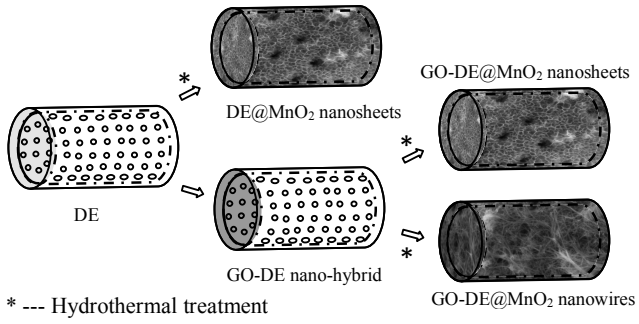

Figure. 1 Schematic diagram presenting the process of synthesis of the as-prepared samples in this work.

MnO_2 structures including nanosheets and nanowires in order to explore the influence of their morphology on supercapacitor performance. The structural, chemical and crystal structure composition of prepared composites were characterized by series of characterization techniques including SEM, XRD, Raman. Their supercapacitor performnaces were characterized by testing capacitance, cycling stability, etc.

Experimental

Materials and reagents

The purified diatom samples is supplied from Mount Sylvia Diatom Pty Ltd (Queensland, Australia). The GO-DE nano-hybrid is prepared by immobilization of graphene nanosheets on purified DE microparticles as described in our pervious work [23]. All the chemicals reagents in analytical purity were purchased from Alfa Aesar.

Sample preparation

GO-DE@MnO_2 Composite with MnO_2 Nanosheets. The GO-DE@MnO_2 composite with MnO_2 nanosheets were prepared by the hydrothermal method. In a typical synthesis, 40 mg of the GO-DE nano-hybrid was dispersed into the $KMnO_4$ solution (30 mL, 0.05 M). The mixed solution was poured into a 50-mL autoclave, and put into an oven for hydrothermal treatment (160 ^oC). After being cooled to room temperature, the precipitate was collected by centrifugation, washed with deionized water, and then dried at 60 ^oC for 6 h, thus obtaining the GO-DE@MnO_2 compostie with MnO_2 nanosheets.

DE@MnO_2 Composite with MnO_2 Nanosheets. The DE@MnO_2 compostie with MnO_2 nanosheets were obtained using the hydrothermal method. Typically, 30 mg of the DE powders were dispersed into the $KMnO_4$ solution (30 mL, 0.05 M).Continuedly, the mixed solution was poured into the autoclave which was then put into an oven for hydrothermal treatment (160 ^oC). After the similar centrifugation procedure, the DE@MnO_2 compostie with MnO_2 nanosheets were obtained.

GO-DE@MnO_2 Composite with MnO_2 Nanowires. The GO-DE@MnO_2 composite with MnO_2 nanowires were prepared from the low-temperature hydrothermal method. Firstly, 0.21 g of the GO-DE nano-hybrid was dissolved in 30 mL of deionized water in a 100-mL beaker, and 2.212 g of $(NH_4)_2S_2O_8$ and 1.85 g of $KMnO_4$ were then added under constant magnetic stirring. The mixture was poured into autoclave, and the autoclave was put into an oven for hydrothermal treatment at 90 ^oC for 12 h. Similarly, the GO-DE@MnO_2 compostie with MnO_2 nanowires were obtained.

Characterization methods

The morphology and structure of as-prepared nanostructures was characterized by focused ion beam scanning electron microscopy (Zeiss Auriga FIB/SEM). The crystal structures of the samples were recorded on powder X-ray diffraction (XRD, Rigaku D/max 2500, Cu Kα). Raman measurements were performed by using a Renishaw (The United Kingdom) inVia micro-Raman spectroscopy system, equipped with 532nm DPSS laser excitations (50mw). A Leica microscope with 50× objective was employed to focus the incident laser on the samples for collection of back-scattered Raman signals. Before the Raman spectra were measured, the wave number of the Raman band of silicon at 520 cm^{-1} was calibrated. The spectral range was from 400 cm^{-1} to 2000 cm^{-1}, the acquisition time of each spectrum was fixed at 10 s, and power on the sample was 1% of the laser power.

Electrochemical measurements

The electrochemical tests of the as-prepared nanostructures were conducted using an electrochemical workstation (CHI 660E) in a three-electrode electrochemical cell with 1 M Na_2SO_4 aqueous solution as the electrolyte. The platinum plate and the saturated calomel electrode (SCE) were used as the counter electrode and the reference electrode, respectively. The working electrodes were prepared by the mixture of active materials, acetylene black and polyvinylidene difluoride (PVDF) in a mass ratio of 7:2:1, which was pasted on the nickel foam. Then the electrodes were dried at 120 ^oC under vacuum. The cyclic voltammetry (CV) tests of the positive electrodes were obtained in the potential range between 0.2 V and 0.8 V by varying the scan rate from 2 and 50 mV s^{-1}. Galvanostatic charge-discharge (CC) experiments were performed with current densities which ranged from 0.25 to 10 A g^{-1} in the same potential range as the CV tests. The electrochemical impedance spectroscopy (EIS) was conducted in the frequency range between 100 kHz and 0.01 Hz with a perturbation amplitude of 5 mV versus the open-circuit potential. The charge-discharge cycling was performed by 2000 cycles at a current density of 2 A g^{-1}.

Results and discussion

The typical SEM image of the GO-DE nanohybrids presents that the surface of DE microparticles is decorated by GO attachment (See supplementary information, Fig. S1). The XRD pattern of the GO-DE (Fig. S2) shows that the weak diffraction peak at 10.834 ^{o} and the sharp diffraction peak of at 27.237 ^{o}, corresponding to the (111) crystal planes of GO and the (331) crystal planes of graphite (JCPDS card no.82-0505). Raman spectra of GO-DE nanohybrid (Fig. S3) displays two characteristic peaks of GO (*i.e.* G: ~1350 cm^{-1} and D: ~1590 cm^{-1}), providing further evidence for the attachment of GO onto the diatom [22,23].

The GO-DE nano-hybrids were of porous structure with uniform and ordered distributions. Utilizing the GO-DE nano-hybrid as a hard template, GO-DE@MnO_2 composite with MnO_2 nanosheets are obtained by tuning hydrothermal treatment (at 160 ^oC for 6 h, 12 h, and 24 h, Fig. 2). Decoration of MnO_2 nanosheets on the surface of the GO-DE composites are in-situ reaction and directional growth process [3]. SEM images clearly show with the increase of processing time from 6 to 24 h, the MnO_2 nanosheets layers become apparently thicker and denser. Furthermore, the magnified images of the GO-DE@MnO_2 (Fig. 2b, d and f) exhibit that the MnO_2 nanosheets are well immobilized on the GO-DE surface. Importantly, the luxuriant ultrathin MnO_2 nanosheets are interconnected to each other, forming a highly porous surface morphology. The unique feature of the MnO_2 nanosheets could increase the specific surface area so as to make more electrical contact with the current collector, which may result in better charge

transfer kinetics and an enhancive electrochemical capacity [12]. In addition, to explore influence of MnO_2 shapes the GO-DE@MnO_2 composite with MnO_2 nanowires was prepared and it can be clearly observed on SEM images presented Fig 3.

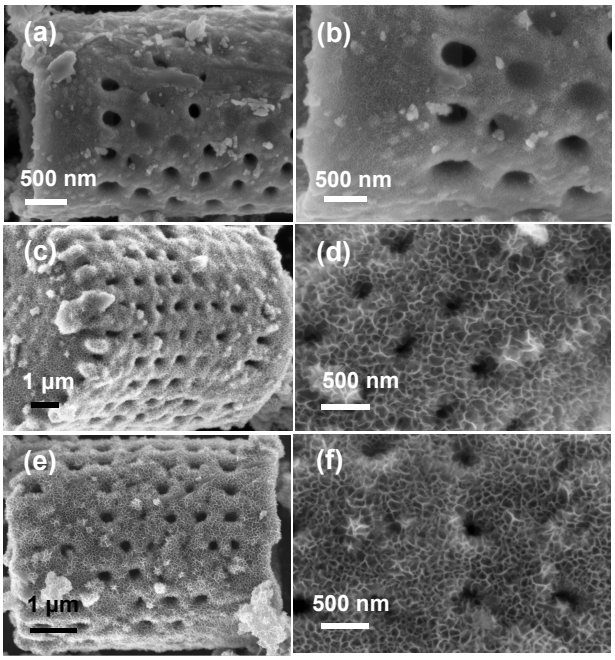

Figure. 2 SEM images of the GO-DE@MnO_2 composite with MnO_2 nanosheets showing the changes of surface morphology of single DE microstructure prepared with different conditions: at 160 °C for (a,b) 6 h, (c,d) 12 h, (e,f) 24 h.

XRD pattern of the GO-DE@MnO_2 composite with MnO_2 nanosheets is depicted in Fig. 4a, which demonstrates that the diffraction peaks at 24.8° and 76.8° correspond to the (011) and (-313) crystal planes of SiO_2 (JCPDS card no.82-1575), and the diffraction peaks at 12.7°, 36.6°, 37.6° and 65.5° match with the (110), (400), (121) and (002) crystal planes of MnO_2 (JCPDS card no.72-1982). Additionally, it could also indicate the weak diffraction peak at 10.7° corresponding to the (111) crystal planes of GO, and the diffraction peak at 20.6° and 27.2° corresponding to the (311) and (331) crystal planes of graphite (JCPDS card no.82-0505). Meanwhile, the weak diffraction peaks of GO and graphite can testify the existence of them, but their contents are less.

Comparatively, the XRD pattern of the DE@MnO_2 composite with MnO_2 nanosheets (Fig. 4b) shows that the diffraction peaks at 22.0 °, 28.4 ° and 31.5 ° could be assigned to the (101) (111) and (102) planes of crystalline SiO_2 with the cristobalite structure (JCPDS card no. 39-1425), confirming a high degree of crystallinity [12,25]. The rest of the diffraction peaks of 12.5 °, 25.2 °, 37.0 °,56.820 ° and 66.2 ° are in great agreement with the (001), (002), (-111), (211) and (020) (JCPDS card no. 80-1098) [10]. Semblably, XRD pattern of GO-DE@MnO_2 composite with nanowires (Fig. 4c) demonstrates the diffraction peaks at 12.7°, 18.1°, 27.4°, 37.6°,42.0°,49.9°, 56.2°, 60.2°, 65.5°, 69.6° and 73.1° corresponding to the (110), (200), (310), (121), (301), (411), (600), (521), (002), (451) and (312) crystal planes of α-MnO_2 (JCPDS card no. 72-1982) [24]. We also observe the diffraction peaks at 21.9°, 31.4°, 36.1° and 77.9°, corresponding to the (101), (102), (200) and (401) crystal planes of SiO_2 (JCPDS card no. 76-0935), and the diffraction peaks at 10.9° of GO and the diffraction peaks at 20.9° of graphite (JCPDS card no. 79-1715).

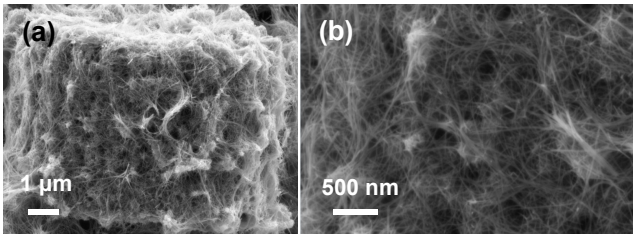

Figure 3 SEM images of the GO-DE@MnO_2 composite with MnO_2 nanowires after hydrothermal treatment at 90 °C for (a,b) 12 h.

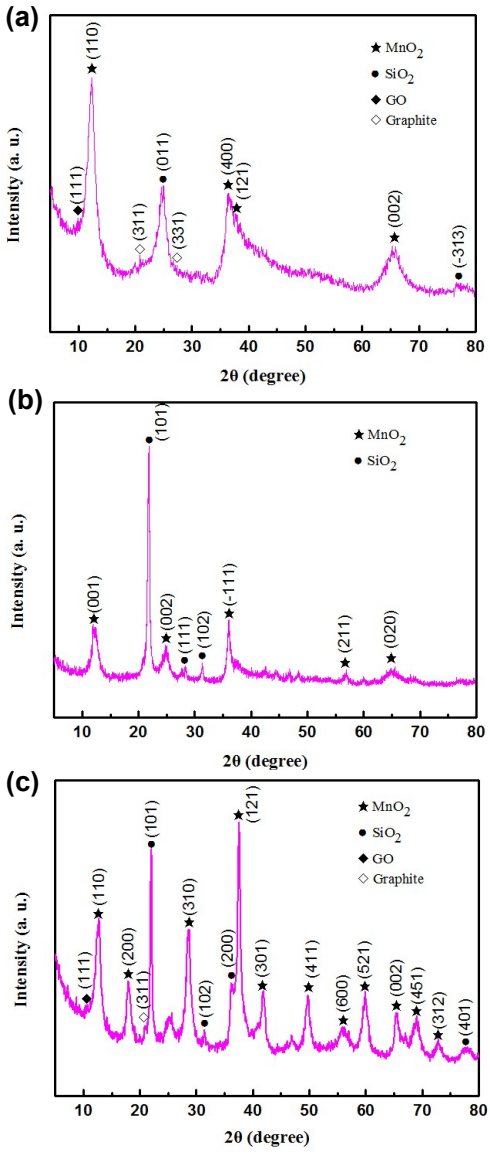

Figure. 4 XRD patterns of (a) the GO-DE@MnO_2 composite with MnO_2 nanosheets obtained at 160 °C for 12 h, (b) the DE@MnO_2 composite with MnO_2 nanosheets obtained at 160 °C for 12 h and (c) the GO-DE@MnO_2 composite with MnO_2 nanowires at 90 °C for 12 h.

Furthermore, XPS measurement was conducted to evaluate the composition of these composites (Fig. S4).

Fig. 5a demonstrates the Raman spectra of the GO-DE@MnO_2 decorated with nanosheets include the weak peak at 577 cm^{-1} and the sharp peak at 656 cm^{-1}, which are well consistent with the vibrational features of the birnessite-type MnO_2 [29]. As shown in Fig. 5b, two distinct peaks located at 574 cm^{-1} and 641 cm^{-1} in the Raman spectra of the GO-DE@MnO_2 decorated with nanowires are assigned to the MnO_2 nanowires. It's surprising that there are no distinct D and G bands in the two Raman spectras. The reason might be that the content of GO is very low conpared with the MnO_2 covered on the top of the surface.

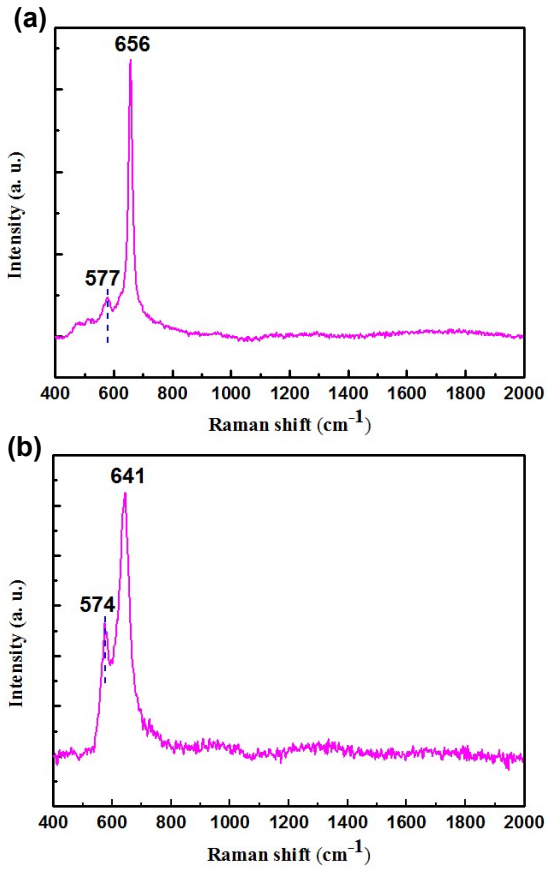

Figure. 5 Raman spectroscopy plots of (a) the GO-DE@MnO_2 composite with MnO_2 nanosheets obtained after hydrothermal treatment at 160 °C for 12 h, (b) the GO-DE@MnO_2 composite with MnO_2 nanowires after hydrothermal treatment at 90 °C for 12 h.

The CV curves of the GO-DE@MnO_2 composites with MnO_2 nanosheets at the scan rate of 50 mV s^{-1} display a typical capacitive behavior without obvious redox peak in the chosen voltage range (Fig. 6a). The CV curve of the GO-DE@MnO_2 composite with MnO_2 nanosheets obtained at 160 °C for 12 h manifests an approximately rectangular shape with a slight deformation, while the CV curves of the composite with nanosheets structures obtained at 160 °C for 6 h and 24 h are of more deformation with a smaller area. The reason might be that the GO-DE@MnO_2 composite with MnO_2 nanosheets obtained at 160 °C for 6 h possesses the thiner, shorter and sparser MnO_2 nanosheets which reduce the specific surface area. Contrarily, the GO-DE@MnO_2 composite obtained at 160 °C for 24 h have too thick MnO_2 nanosheets which have entirely blocked the pores on the surface GO-DE@MnO_2 hindered effective transport of the electrolyte ions. More or less, the ideal rectangular shape of the MnO_2 nanosheets obtained at 160 °C for 12 h indicated the ideal electrochemical pseudo-capacitive behavior of the electrode.

The galvanostatic charge-discharge curves of the GO-DE@MnO_2 composites decorated with nanosheets at the same current density of 0.5 A g^{-1} are depicted in Fig. 6b. As we can see, the charging curves are almost symmetric to its corresponding discharging counterpart, indicating that the samples have good electrochemical performance and reversibility. The specific capacitances of these composites with MnO_2 nanosheets obtained at different conditions (160 °C for 6, 12 and 24 h) are calculated to be 136.9, 152.5 and 138.5 F g^{-1} at the current density of 0.5 A g^{-1} respectively, displaying the specific capacitance of the as-prepared samples at various current densities (Fig. 6c).

EIS measurements of the GO-DE@MnO_2 composites decorated with MnO_2 nanosheets were performed in the frequency range from 0.01 to 100 kHz, as shown in Fig. 6d. It can be seen that the Nyquist plots of the three profiles are similar in shape, composed of partial semicircle at high frequency and a linear component in the low frequency region. The semicircle in the high-frequency range is associated with the charge-transfer resistance (R_{ct}), and a nearly 90 ° of the vertical line at low frequency is observed, indicating an ideal capacitive behavior of electrochemical double-layer capacitor [26-28]. From the inset in Fig. 6d, the R_{ct} values of composites with MnO_2 nanosheets obtained at 160 °C for 6 h, 12 h and 24 h are estimated to be about 6.3, 6.6 and 7.7 Ù, respectively. The cycle stability was further evaluated by repeating the CV measurements at

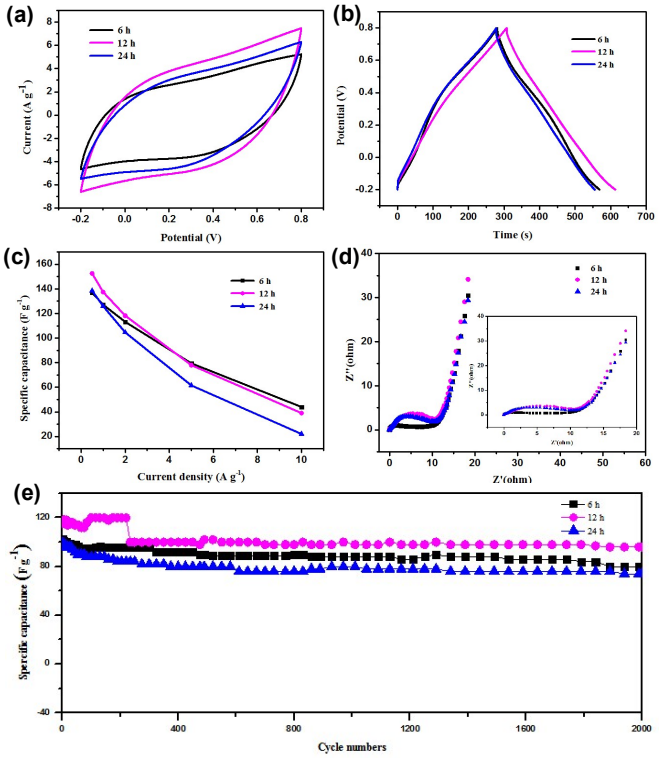

Figure. 6 The electrochemical performance of the GO-DE@MnO_2 nanosheets electrodes measured in 1 M Na_2SO_4 solution. (a) CV curves measured at a scan rate of 50 mV s^{-1}. (b) Galvanostatic charge-discharge

curves at the current density of 0.5 A g^{-1}. (c) Specific capacitance at various current densities. (d) Electrochemical impedance spectrum at open circuit potential in the frequency range from 0.01 Hz to 100 kHz. (e) Cycling performance at the current density of 2 A g^{-1}.

the current density of 2 A g^{-1} for 2000 cycles, as depicted in Fig. 6e. The percentage of 78.1%, 83.3%, and 74.3% of the original capacitance is reserved for the GO-DE@MnO_2 composite with nanosheets obtained at 160 °C for 6 h, 12 h and 24 h, respectively, signifying good electrochemical stability as the supercapacitor electrode material.

The comparison of electrochemical performances of DE@MnO_2 and GO-DE@MnO_2 both with MnO_2 nanosheets is displayed in Fig. 7. Fig. 7a shows that GO-DE@MnO_2 with nanosheets morphology displays a higher integrated area than that for DE@MnO_2 composite with nanosheets at the same scan rate, signifying excellent electrochemical performance for the GO-DE@MnO_2 composite with nanosheets. Fig. 7b presents the galvanostatic charge-discharge curves of DE@MnO_2 and GO-DE@MnO_2 composites with nanosheets at the same current density of 0.5 A g^{-1}, which show good symmetrical linear curves. There is no doubt that the specific capacitance of GO-DE@MnO_2 composite with MnO_2 nanosheets electrode is higher than that of DE@MnO_2 nanosheets electrode, which are calculated for 152.5 and 52.8 F g^{-1}, respectively. Fig. 7c also testifies the importance of the GO attachment, which is beneficial to the ion diffusion between the electrolyte and the active material.

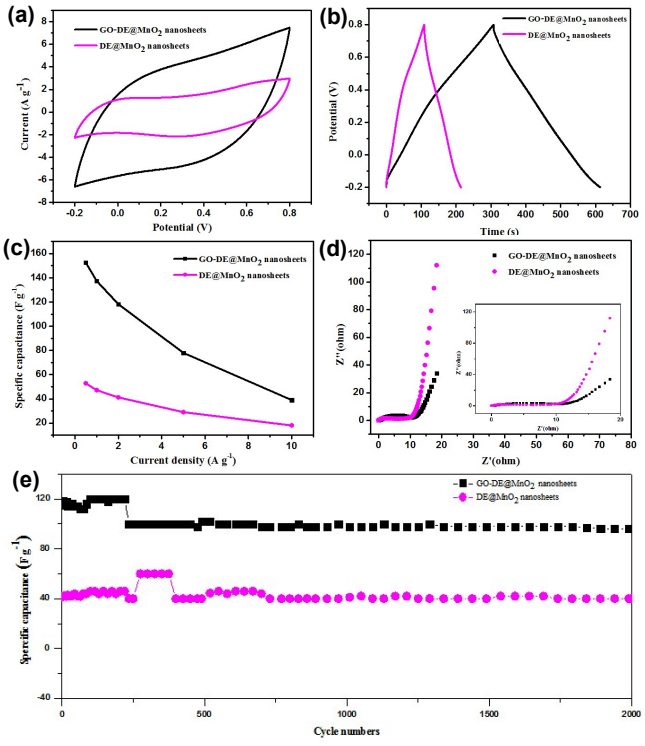

Figure. 7 The electrochemical performance of the GO-DE@MnO_2 composite electrode decorated with nanosheets and the DE@MnO_2 composite nanosheets electrodes measured in 1 M Na_2SO_4 solution. (a) CV curves measured at a scan rate of 50 mV s^{-1}. (b) Galvanostatic charge-discharge curves at a current density of 0.5 A g^{-1}. (c) Specific capacitance at various current densities. (d) Electrochemicalimpedance spectrum at open circuit potential in the frequency rangefrom 0.01 Hz to 100 kHz. (e) Cycling performance at the current density of 2 A g^{-1}.

The Nyquist plots (Fig. 7d) of GO-DE@MnO_2 and DE@MnO_2 composite decorated with MnO_2 nanosheets consist of a semicircle with the charge-transfer resistance (R_{ct}) between electrolyte and electrode at high frequency range and the almost straight line in the low frequency region, which is related to ion diffusion to the electrode [26]. Fig. 7e shows that the cycle stability of the DE@MnO_2 nanosheets was measured by repeating the CV measurements at the current density of 2 A g^{-1} for 2000 cycles as well, and 95.2% of the original capacitance is retained.

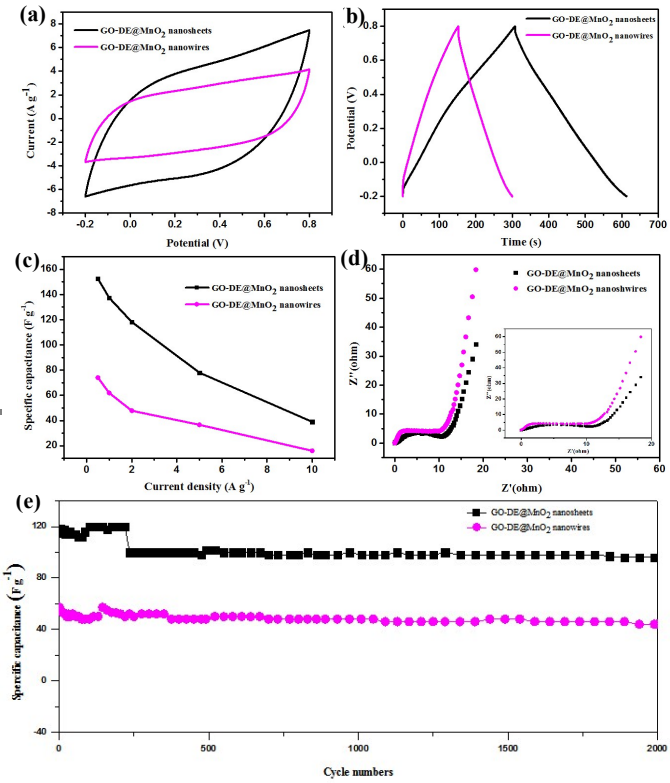

Figure. 8 The electrochemical performance of the GO-DE@MnO_2 composite electrode decorated with MnO_2 nanosheets and the DE-GO-MnO_2 composites electrode with MnO_2 nanowires measured in 1 M Na_2SO_4 solution. (a) CV curves measured at a scan rate of 50 mV s^{-1}. (b) Galvanostatic charge-discharge curves at a current density of 0.5 A g^{-1}. (c) Specific capacitance at various current densities. (d) Electrochemical impedance spectrum at open circuit potential in the frequency rangefrom 0.01 Hz to 100 kHz. (e) Cycling performance at the current density of 2 A g^{-1}.

Fig. 8a exhibits that the GO-DE@MnO_2 composite with nanosheets electrode displays a higher integrated area compared with DE@MnO_2 composite with nanowires at the same scan rate. Fig. 8b and c present that the specific capacitance of GO-DE@MnO_2 composite with nanowires is calculated to be 74.0 F g^{-1}. Apparently, the GO-DE@MnO_2 composite with nanosheets with higher specific capacitance have more potential for the supercapacitor electrode, which may be ascribed to birnessite crystal structure and larger specific surface area of the GO-DE@MnO_2 composite with MnO_2 nanosheets. In addition, the EIS measurements of the GO-DE@MnO_2 composite with MnO_2 nanowires was performed in the frequency range from 0.01 to 100 kHz demonstrated in Fig. 8d, and the R_{ct} value of the GO-DE@MnO_2 composite with MnO_2 nanowires is about 7.6 Ù. Fig. 8e shows the cycle stability of the DE@MnO_2 composite with MnO_2 nanowires and GO-DE@MnO_2 composite

with MnO_2 nanosheets measured by repeating the CV measurements at the current density of 2 A g^{-1} for 2000 cycles, and 62.9% of the original capacitance is retained for DE@MnO_2 composite with MnO_2 nanowires.

Conclusions

In summary, the nano-hybrid composite materials based natural 3D diatom silica microparticles, 2D GO sheets (GO-DE nano-hybrid) and MnO_2 nanostructures were synthesized for the first time. A series of electrochemical tests were performed to investigate the electrochemical properties of the GO-DE@MnO_2 composites with MnO_2 nanosheets and nanowires morphologies, as the supercapacitor electrodes. Our results showed that the GO-DE@MnO_2 composites with MnO_2 nanosheets surface morphology obtained at 160 ^oC for 12 h presented the larger specific capacitance of 152.5 F g^{-1} and the relatively better cycle stability (83.3% capacitance retention after 2000 cycles). The presented results also suggest that the MnO_2-modified 3D GO-DE composites based on unique diatom silica structures samples have great prospects to be active material for cost-effective, flexible, and electrochemically stable supercapacitors.

Acknowledgements

The authors gratefully acknowledge the financial supports provided by National Natural Science Foundation of China (Grant no. 51104194 and 61474011), International S&T Cooperation Projects of Chongqing (CSTC2013gjhz90001), National Key laboratory of Fundamental Science of Micro/Nano-device and System Technology (2013MS06, Chongqing University), Laboratory of Precision Manufacturing Technology, CAEP (KF13004), State Education Ministry and Fundamental Research Funds for the Central Universities (Project no. CDJZR14135501, Chongqing University, PR China).

References

1 D. Qu, L. Wang, D. Zheng, L. Xiao, B. Deng, D. Qu, *Journal of Power Sources*, 2014, **129–135**, 269.
2 S. Wang, C. Jin, W. Qian, *Journal of Alloys & Compounds*, 2014, **12–17**, 615.
3 W. Wang, Q. Hao, W. Lei, X. Xia, X. Wang, *Journal of Power Sources*, 2014, **250–259**, 269.
4 Z. Fan, J. Yan, T. Wei, L. Zhi, G. Ning, T. Li, *Advanced Functional Materials*, 2011, **2366–2375**, 21.
5 Y. Chen, L. Du, P. Yang, P. Sun, X. Yu, W. Mai, *Journal of Power Sources*, 2015, **68–74**, 287.
6 G. Xin, Y. Wang, X. Liu, J. Zhang, Y. Wang, *Electrochimica Acta.*, 2015, **254–261**, 167.
7 X. Feng, Z. Yan, N. Chen, Y. Zhang, X. Liu, Y. Ma, X. Yang, W. Hou, *New Journal of Chemistry*, 2013, **2203-2209**, 37.
8 X. Feng, N. Chen, Y. Zhang, Z. Yan, X. Liu, Y. Ma, Q. Shen, L. Wang, W. Huang, *Journal of Material Chemistry A*, 2014, **9178-9184**, 2.
9 M. Huang, Y. Zhang, F. Li, L. Zhang, R. Ruoff, Z. Wen, *Scientific Reports*, 2014, **3878**, 4.
10 X. Zhang, P. Yu, H. Zhang, D. Zhang, X. Sun, Y. Ma, *Electrochimica Acta.*, 2013, **523–529**, 89.
11 J. Ma, S. Zhu, Q. Shan, S. Liu, Y. Zhang, F. Dong, *Electrochimica Acta.*, 2015, **97–103**, 168.
12 F. Li, Y. Xing, M. Huang, L. Li, T. Yu, Y. Zhang, L. Dusan, *J. Mater. Chem. A.*, 2015, **7855**, 3.
13 C. Zhao,K. Shu, C. Wang, S. Gambhir, G. Wallace, *Electrochimica Acta.*, 2015, **12-19**, 172.
14 J. Chen, Y. Liu, W. Li, C. Wu, L. Xu, H. Yang, *Journal of Materials Science*, 2015, **5466-5474**, 16.
15 X. Feng, Z. Yan, N. Chen, Y. Zhang, Y. Ma, X. Liu, Q. Fan, L. Wang, W. Huang, *Journal of Material Chemistry A*, 2013, **12818-12825**, 1.
16 J. Li, H. Xie, Y. Li, *Journal of Nanoscience&Nanotechnology.*, 2015, **3280-3283**, 15.
17 Q. Qu, P. Zhang, B. Wang, Y. Chen, S. Tian, Y. Wu, *J. Phys. Chem. C.*, 2009, **14020–14027**, 113.
18 X. Tang, Z. Liu, C. Zhang, Z. Yang, Z. Wang, *Journal of Power Sources*, 2009, **939-943**, 193.
19 J. Kang, A. Hirata, L. Kang, X. Zhang, Y. Hou, L. Chen, *Angewandte Chemie International Edition.*, 2013, **1708-1711**, 52.
20 L. Qiang, J. Liu, J. Zou, A. Chunder, Y. Chen, Z. Lei, *Journal of Power Sources*, 2011, **565–572**, 196.
21 S. Zhu, W. Cen, L. Hao, J. Ma, L. Yu, H. Zheng, *Materials Letters.*, 2014, **11–14**, 135.
22 G. Liu, L. Fan, F. Yu, J. Wu, L. Lu, Z. Qiu, *Journal of Materials Science*, 2013, **8463-8470**, 48.
23 T. Kumeria, M. Bariana, T. Altalhi, M. Kurkuri, T. Gibson, W. Yang, L. Dusan, *J. Mater. Chem. B.*, 2013, **6302-6311**, 1.
24 Y. Du, G. Zheng, J. Wang, L. Wang, J. Wu, H. Dai, *Microporous & Mesoporous Materials*, 2014, **27–34**, 200.
25 Y. Zhang, M. Huang, F. Li, X. Wang, Z. Wen, *Journal of Power Sources*, 2014, **449-456**, 246.
26 L. Yan, Y. Xu, M. Zhou, G. Chen, S. Deng, S. Smirnov, *Electrochimica Acta.*, 2015, **73–81**, 169.
27 G. Sun, B. Li, J. Ran, X. Shen, H. Tong, *Electrochimica Acta.*, 2015, **13–22**, 171.
28 D. Antiohos, K. Pingmuang, M. Romano, S. Beirne, T. Romeo, P. Aitchison, *Electrochimica Acta.*, 2013, **99–108**, 101.
29 M. Huang, R. Mi, H. Liu, F. Li, X. Zhao, W. Zhang, S. He, Y. Zhang, *Journal of Power Sources*, 2014, **760–767**, 269.

Graphical abstract